Predicting Spectral Parameters in the Backscattering-dominated Model for the Prompt Phase of GRBs

Mukesh K. Vyas[1] , Asaf Pe'er[1] , and David Eichler[2]
[1] Bar Ilan University, Ramat Gan, 5290002, Israel; mukeshkvys@gmail.com
[2] Ben-Gurion University, Be'er Sheva, 84105, Israel

Abstract

We present new results of the backscattering-dominated prompt emission model in which the photons generated through pair annihilation at the center of a gamma-ray burst (GRB) are backscattered through Compton scattering by an outflowing stellar cork. Using a Comptonized pair annihilation spectrum accompanied by bremsstrahlung radiation for seed photons, we show that the obtained spectra produce a low-energy photon index in the range $\alpha \sim -1.95$ to -1.1, steeper high-energy slopes $\beta \sim -3.5$ to -2.4, and spectral peak energies approximately a few KeV to a few tens of MeV. These findings are consistent with the values covered in GRB prompt phase observations.

Unified Astronomy Thesaurus concepts: High energy astrophysics (739); Gamma-ray bursts (629); Relativistic jets (1390); Theoretical models (2107)

1. Introduction

In the current understanding of long gamma-ray bursts (GRBs), a collapsing core of a massive star (e.g., a Wolf–Rayet star) leads to the observed GRB phenomenon (Levinson & Eichler 1993; Woosley 1993a; MacFadyen & Woosley 1999), while two compact stars gravitationally merge to produce a short GRB. In both the cases, a double-sided jet is produced from the center of the burst. As it propagates through the envelope of the collapsing star, this jet collects material ahead of it thereby forming a dense stellar cork that expands ahead of it. This cork is less energetic in short GRBs compared to long GRBs (Nakar & Piran 2017). After crossing the stellar envelope, the jet eventually pierces through the cork and escapes the system (Ramirez-Ruiz et al. 2002; Zhang et al. 2003, 2004; Nagakura et al. 2014). Energetic electrons inside the jet produce the observed signal responsible for the GRB prompt phase. The observed spectrum is often interpreted in the framework of synchrotron radiation (Meszaros et al. 1993; Tavani 1996; Pilla & Loeb 1998; Kumar & Zhang 2015; Pe'er 2015).

An alternate picture of the prompt phase was proposed and developed by Eichler & Manis (2008), Eichler (2014, 2018), and Vyas et al. (2021) according to which most of the photons are produced at the center of the star near the time of the burst through pair annihilation, in a plasma dominated by $e^{\pm}$ pairs. Pair annihilation in this plasma naturally produces a radiation pattern having an equilibrium temperature around a few MeV (Goodman 1986; Paczynski 1986; Eichler 2014, 2018). The cork in this picture, after being pushed by the expanding gas and radiation pressure, moves with relativistic speed ahead of the radiation beam emitted by the pair plasma. The radiation beam is not able to pierce through it, and most of the photons are reflected backward. Due to the relativistic aberration, these photons are beamed toward the motion of the cork before being detected by the observer.

In previous attempts of incorporating Comptonization in the GRB atmosphere, Brainerd (1994) assumed a power-law spectrum as seed photons' distribution and studied its attenuation through the medium assumed above the burst. He explained spectral features of the burst including the spectral peak energies. Daigne et al. (2011) assumed that the seed photons have a synchrotron spectrum and studied its modification due to Compton scattering in the burst atmosphere. Compared to these works, here we do not consider synchrotron or nonthermal power-law process. Rather, our setup assumes a thermal (Maxwellian) distribution of pairs that emit photons via annihilation in the inner region of an empty jet funnel. An annihilation spectrum intrinsically has bremsstrahlung contribution, and the photons are Comptonized within the pair plasma to produce the final seed spectrum. These photons then propagate through the jet funnel, after which they interact with the outflowing cork, producing the observed prompt GRB signal. As we show below, the obtained spectrum has a negative low-energy photon index. Further, power laws at high energy are generated due to multiple Compton scattering of the seed photons inside the cork. In Vyas et al. (2021, hereafter VPE21), we showed that multiple scattering of photons inside the cork that scattered from different angles with respect to the observer can explain some key observations such as the Amati correlation (a correlation between spectral peak energies $\varepsilon_{\text{peak}}$ and equivalent isotropic energies ε_{iso}; see Amati 2006; Farinelli et al. 2021) and spectral lag, which could not be addressed in other works.

However, following the assumption of monoenergetic seed photons, the obtained low-energy slopes in VPE21 were positive and hence deviating compared to the observed slopes. In this Letter, we resolve this problem by considering Comptonized pair annihilation spectra for the seed photons at the center of the burst as explained above. With this modification, the typical magnitudes of obtained low-energy spectra are consistent with observations.

In Section 2 we briefly describe the model and proceed to detail the assumed electron–positron pair annihilation spectrum for seed radiation field in Section 3. We discuss the results in Section 4 before summarizing the Letter in Section 5.

2. Brief Picture of the Backscattering-dominated Model

Near the centre of the burst, the seed photons are produced by pair annihilation and bremsstrahlung. These photons are further Comptonized by the local plasma present there. The detailed process of which is described in Section 3. These photons propagate inside the empty jet funnel to radially enter
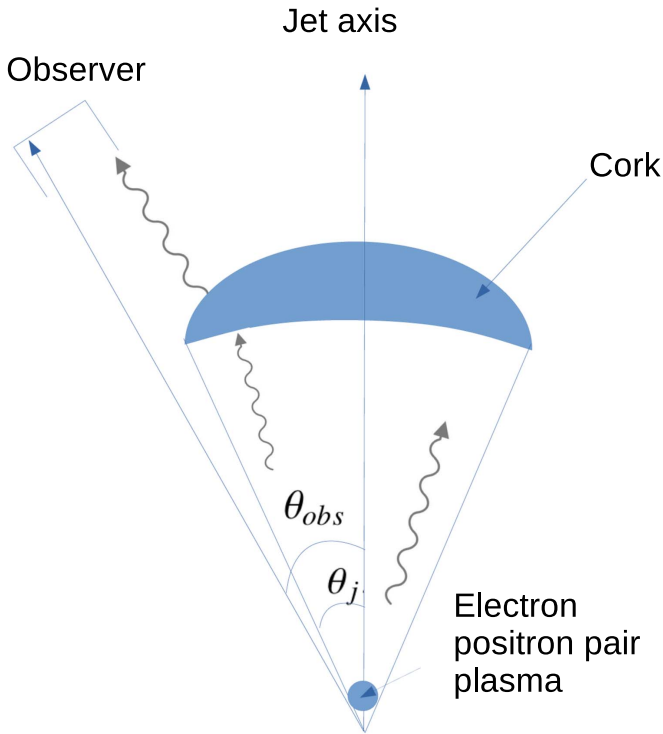
Figure 1. Geometry of the system. Source of the radiation is electron–positron pair plasma producing an annihilation spectrum at the center of the burst. The photons enter the cork that expands with Lorentz factor γ and temperature T_c. The opening angle of the jet (and cork) is θ_j, while the observer, situated at θ_{obs}, observes photons that are scattered backward by the inner surface of the cork.

an optically thick cork with an opening angle θ_j. The cork adiabatically expands with a constant Lorentz factor γ and temperature T_c at initial distance r_i from the center of the star (Figure 1). We carry out Monte Carlo simulations for studying the interaction of these photons with the relativistic electrons inside the cork. These photons may go through multiple Compton scattering with the energetic electrons before escaping through the cork's back surface. If the photons do not escape within 25 scatterings, we consider them to be lost inside. Following the relativistic motion of the cork, all escaped photons are relativistically beamed in the forward direction and a fraction of these photons is observed by an observer situated at an angle $\theta_{\rm obs}$ from the jet axis and at azimuth $\phi_{\rm obs}$. The detected photons thus produce a spectral as well as a temporal evolution (light curve). Here, θ and ϕ are the spherical coordinates measured from the center of the star. The system possesses azimuthal or ϕ symmetry. We extend the work of VPE21, considering a relativistic Comptonized electron–positron pair annihilation spectrum with temperature T_r as a source of seed photons, and reproduce the spectra. Other details of the model are identical to those given in VPE21.

3. Seed Photon Distribution: Comptonized Pair Annihilation Spectrum

In a collapsing star, free neutrinos are generated and annihilate near the center of the star in an empty funnel behind the outflowing jet. The neutrino annihilation near the center of the star produces a copious amount of electron–positron (e^-e^+) pairs (Woosley 1993b; MacFadyen & Woosley 1999; Popham et al. 1999; Levinson & Eichler 2003; McKinney 2005a, 2005b; Globus & Levinson 2014). The e^-e^+ pairs fall toward the

gravitating center below a stagnation surface due to gravity and they escape outward above it (see, e.g., Figure 1 of McKinney 2005a). This plasma is hot with relativistic temperatures, and the pairs are in equilibrium with radiation produced within the plasma (Levinson & Globus 2013). The pair plasma produces a pair annihilation spectrum and associated bremsstrahlung radiation. This spectrum is further modified due to Compton scattering within the plasma. The emerging spectra that follow bremsstrahlung and Comptonization from thermal distribution of plasma at temperature T_r were studied by Zdziarski (1984) through Monte Carlo simulations. There, he showed that the resultant spectrum at relativistic temperatures is flat in nature and decays exponentially at high frequencies. For a typical plasma with density $n = 2 \times 10^{18}$ cm^{-3}, $\Theta_r = k_B T_r/m_e c^2$, and escape optical depth $\tau = 1$. We obtain the following numerical fit to the respective spectrum integrated over the emitting surface:

$$F_\varepsilon = C_0 \exp\left(-\frac{C_1 \varepsilon^2}{\Theta_r^2}\right) \quad \mathrm{KeV \ s^{-1}/KeV^{-1}}. \tag{1}$$

Here ε is energy of the photons normalized to electron's rest energy $m_e c^2$, k_B is Boltzmann's constant, m_e is the mass of the electron, c is the light speed, and $C_1 = 0.045$. $C_0 (= 2 \times 10^{40}$ KeV s^{-1}/KeV$)$ is a normalization parameter that depends on the pair density. As long as the plasma is relativistic it is independent of T_r. Note that its value does not affect the overall spectral shape, hence its exact parametric dependence will not affect the results presented here. Our Equation (1) provides good fit to the data presented by Zdziarski (1984) in his Figures 1(d) and (e). We find that this fit is applicable for relativistic temperatures $\Theta_r > 0.3$ where the emergent spectra are flat.

These photons, then, propagate and enter the outflowing optically thick cork with temperature $\Theta_c = k_B T_c/m_e c^2$. Further, the outcome of this seed spectrum intrinsically considers a constant temperature Θ_r. It is a reasonable assumption as long as we are considering the prompt phase spectra where only the initial temperature of the pair plasma is important. Thus, we retain the assumption of the delta function in injection time used in the previous paper. Later evolution of Θ_r to lower temperatures, related emission, and their scattering with the cork may contribute to GRB emissions at late times, i.e., afterglows, are beyond the current scope of this Letter.

4. Results

4.1. General Appearance of the Spectrum

The cork forms effectively below the surface of the star with a typical radius $r_s = 10^{10} - 3 \times 10^{12}$ cm. It is accelerated above it reaching an uncertain Lorentz factor that can be a few tens at a distance $r_i \gtrsim r_s$ from the center of the star. Is was shown by Waxman & Mészáros (2003) that the cork may reach terminal Lorentz factor as high as 100 under specific conditions. However, other authors argue that a more typical value of the terminal Lorentz factor is only a few tens (see Zhang et al. 2003; López-Cámara et al. 2013 for details). Hence, lacking a complete theory, in this Letter, we explore the emerging spectra from a range of possible terminal Lorentz factors, $\gamma \sim 10$–100. We further consider the cork to expand radially and lose its energy adiabatically at a distance $r_i = 10^{12.5}$ cm from the center of the star. To generate a typical resultant spectrum, we consider a constant Lorentz factor of the cork $\gamma = 100$, with opening angle $\theta_j = 0.1$ rad and a temperature $\Theta_c = 1.4$. Approximately ~ 26 million photons are
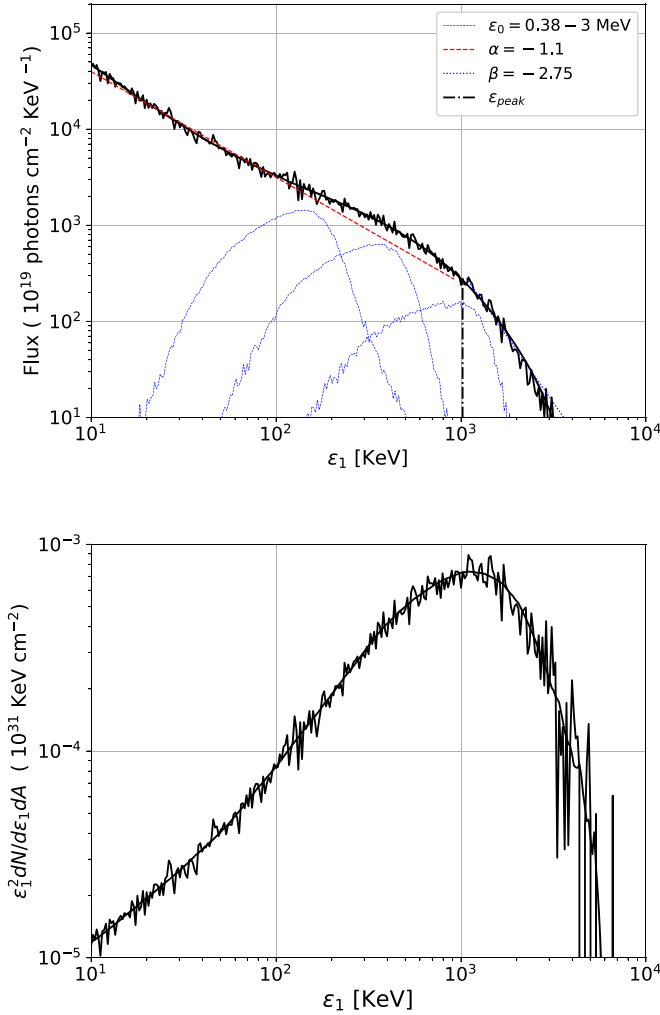
Figure 2. Top panel: photon spectrum (solid black) for $\gamma = 100$ and $\theta_{\mathrm{obs}} = 0.175$ obtained for pair temperature $\Theta_r = 3$. The jet opening angle is $\theta_j = 0.1$ rad. It is fitted for low-energy photon index $\alpha = -1.1$, $\beta = -2.75$. Both the photon indices are connected at spectral peak energy $\varepsilon_{\mathrm{peak}} = 1020$ KeV. Blue dotted curves are corresponding monoenergetic photons for $\varepsilon_0 = 378$, 1000, and 3000 KeV. Bottom panel: corresponding spectral emissivity $\epsilon_1^2 dN/d\epsilon_1$. Overplotted solid black curve in both panels is obtained by applying the Savitzky–Golay filter for data smoothing.

injected in the code and scaled with the burst having energy 10^{50} erg to calculate the fluxes. Hence the spectra are shown in the rest frame of the burst and are independent of cosmic redshift.

In the top panel of Figure 2, the spectrum obtained for seed distribution of Comptonized pair annihilation and bremsstrahlung spectrum (according to Equation (1)) is shown by black solid curve. To explain how this spectrum is generated, we plot the scattered spectra obtained for three different cases of monoenergetic photons, $\varepsilon_0 = 378$, 1000, and 3000 KeV (blue dotted curves); this is the setup considered in VPE21. Here the number of photons at each energy ε_0 are supplied according to the Comptonized pair annihilation spectral distribution of photons $dN/dtd\varepsilon = (F_\varepsilon/\varepsilon)$ in Equation (1). It can be seen that the resulting spectrum is a superposition of the spectra generated by monoenergetic seed photons. The blueshifted peaks represent the increasing values of ε_0. In the bottom panel, corresponding spectral emissivity $\varepsilon^2 dN/d\varepsilon_1 dA$ (KeV cm^{-2}) is plotted. We used the Savitzky–Golay filter to show the nature of the spectra by data

smoothing. The filtered curves are shown by overplotted solid curves in both the spectra. For the parameters used, the spectral peak energy $\varepsilon_{\mathrm{peak}}$ is obtained at 1020 KeV and it separates the two spectral regimes with slopes α and β. All three monoenergetic spectra have positive low-energy photon indices $\alpha = -1$, while the resultant spectrum produces a negative slope $\alpha = -1.1$. The high-energy photon index is obtained to be $\beta = -2.75$. This result is similar to the observational result of the prompt GRB spectra that show $\alpha = -1$ and $\beta = -2.5$ (Kaneko et al. 2006; Pe'er 2015). In our model, generation of power laws at high energy follows from multiple scattering inside the cork; a complete explanation for this part of the spectrum appears in Section 3.2.1 (e.g., Figure 4) of VPE21. The obtained peak energies are also in accordance with the most abundant observed values for redshifted corrected spectra (see Figure 3 of Gruber et al. 2011).

4.2. Parametric Dependence and Explaining the Observed Spectra

The spectrum shown in Figure 2 is generated for specific parameters. Due to the high uncertainty in the theoretical models describing the formation, acceleration, and composition of the cork, there is a high uncertainty in a number of key physical parameters describing the system. We show here that this uncertainty, by large, has only a moderate effect on the observed signal. In this respect, we analyze the dependence of α, β, and $\varepsilon_{\mathrm{peak}}$ on system variables like cork Lorentz factor γ, cork temperature Θ_c, the pair temperature Θ_r, and the observer's angle θ_{obs}.

4.2.1. Dependence of Observed Spectra on Observing Angle θ_{obs}

In the top two panels of Figure 3 we plot respective spectra (flux and spectral emissivity) as seen by different observers situated at different observing positions $\theta_{\mathrm{obs}}(= 0.005–0.355$ rad). All other parameters are kept identical to Figure 2. In the bottom panel, we show the variation of $\varepsilon_{\mathrm{peak}}$ with θ_{obs}. The observer's position does not change the spectral slopes and hence α and β are constant for all the observers situated at different angular positions. However, due to relativistic beaming, the observers at larger angular positions receive less flux as well as the spectral peak becomes softer. Variation of $\varepsilon_{\mathrm{peak}}$ with θ_{obs} is shown in the last panel. For the observers within the jet angle $\theta_j = 0.1$ rad, $\varepsilon_{\mathrm{peak}}$ is roughly constant (a few tens of MeV) while it monotonically decreases for $\theta_{\mathrm{obs}} > \theta_j$ and falls up to a few KeV for $\theta_{\mathrm{obs}} \sim 0.35$ rad.

4.2.2. Spectral Evolution with Cork Lorentz Factors (γ)

In the top panel of Figure 4, we consider three values of $\gamma = 10$, 20, and 100 and plot the spectrum scattered by a cork with temperature $\Theta_c = 0.06$. These spectra are seen by an observer at $\theta_{\mathrm{obs}} = 0.105$ rad. The spectral shape is not very sensitive to γ as the seed photons are first redshifted in the cork frame by a factor of 2γ, and then after backscattering, these are again blueshifted for an on axis observer by the same amount. However, the flux received from less relativistic corks significantly decreases due to less effective relativistic beaming toward the observer. The low-energy photon indices are unaffected by γ. In the bottom panel, we show that the spectra are harder showing smaller magnitudes of β for larger γ. This can be understood as the seed photons transforms to less energy for higher γ and thus these photons are more efficiently inverse
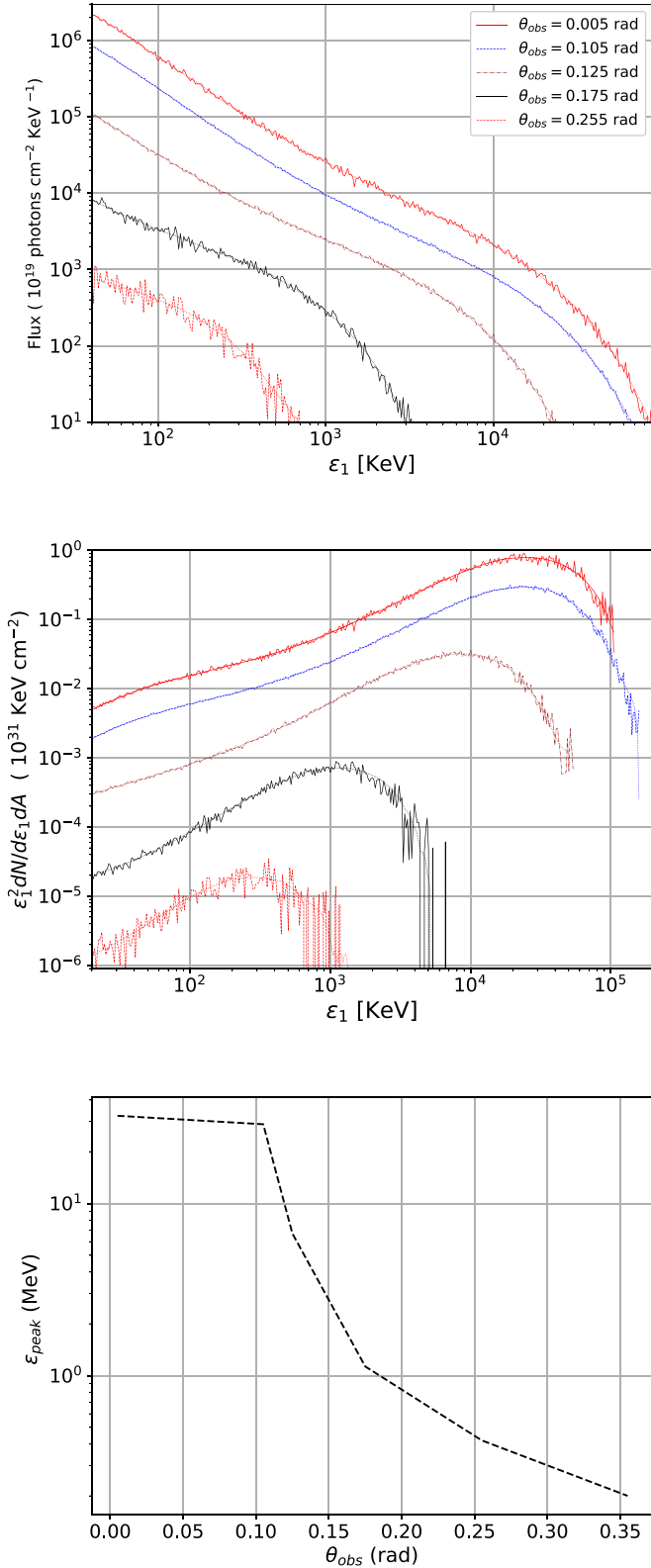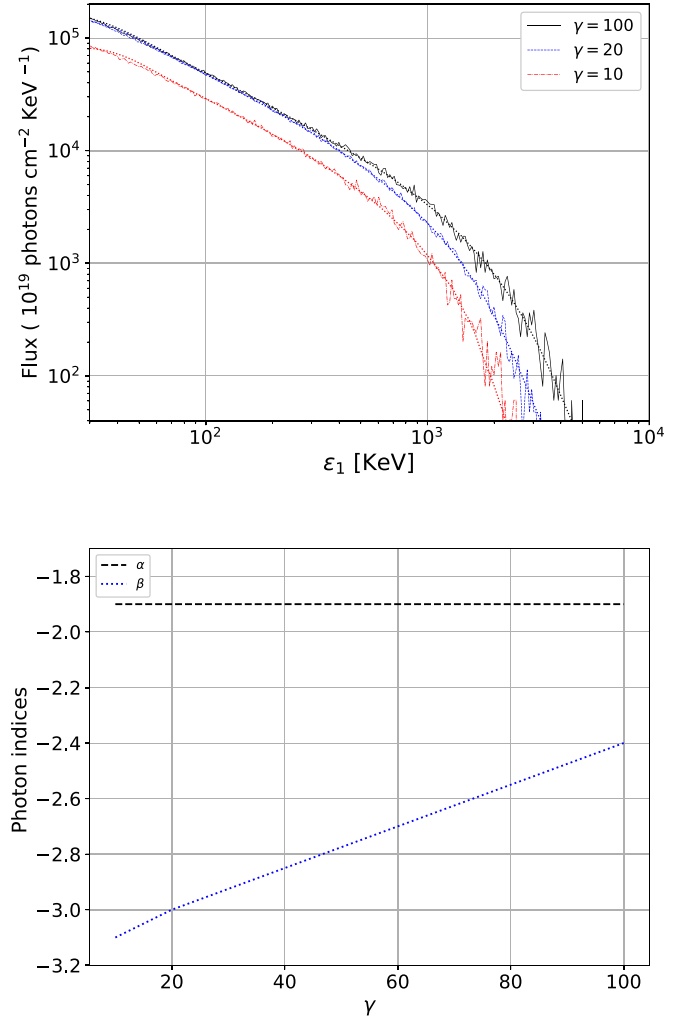
Figure 4. Top panel: spectra for various Lorentz factors $\gamma = 10$, 20, and 100 for the pair temperature $\Theta_r = 3$, cork temperature $\Theta_c = 0.06$, and $\theta_{obs} = 0.105$ rad. Overplotted dotted curves are obtained smoothed data points after applying the Savitzky–Golay filter. Bottom panels: variation of α and β with γ for the same parameters.

4.2.3. Effect of Plasma Temperature Θ_r and Cork Temperatures Θ_c on the Spectra

The spectrum evolves with the seed photons' energy that is governed by pair temperature Θ_r. Corresponding spectral variation is shown in the top left panel of Figure 5 for $\Theta_r = 1$, 3, and 10. Here $\gamma = 20$, $\Theta_c = 0.06$, and $\theta_{obs} = 0.105$ rad. The spectrum gets harder when the plasma assumes higher temperature and subsequently emits more photons at higher energy. In the subsequent panels below the spectra, we plot the variation of α β and ε_{peak} as functions of Θ_r. As Θ_r varies in the range 1–10, α mildly changes from -1.95 to -1.85, β changes from -3.5 to -2.5, while the spectral peak energy ε_{peak} evolves from 102 to 186 KeV.

As the photons lose or gain energy by multiple scattering inside the cork, all the spectral parameters are sensitive to Θ_c. In the top right panel of Figure 5, we show the spectra for different choices of Θ_c in the range 0.06–0.4. Here $\gamma = 20$, $\Theta_r = 3$, and $\theta_{obs} = 0.105$ rad are kept constant. As the electrons are more energetic in the hotter cork, the spectra are harder showing a decrease in magnitudes of α, β and an increase in ε_{peak}, respectively, shown in the bottom panel in the right

Figure 3. Variation of spectra (top and middle panels) with observing angles in the range $\theta_{obs} = 0.005$–0.35 rad. Overplotted dotted curves show the corresponding smoothed spectra by applying the Savitzky–Golay filter. Variation of ε_{peak} with θ_{obs} (bottom panels). Other parameters are the same as in Figure 2.

Comptonized to gain energy inside the cork thereby making the spectrum harder. Variation of γ between 10 and 100 thus produces a range of $\beta = -3.1$ to -2.4.
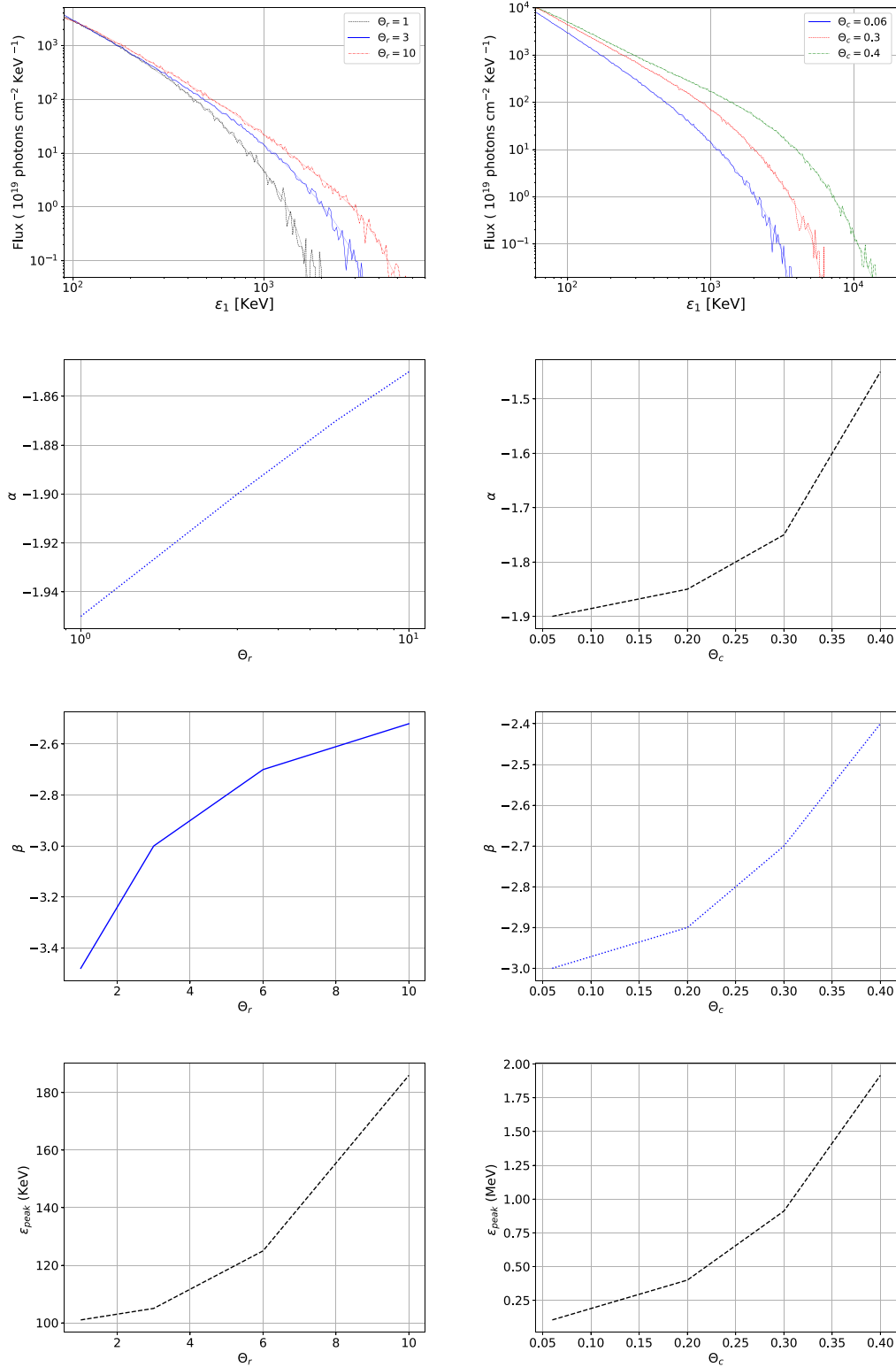
Figure 5. First row: dependence of spectra on various choices of pair temperatures $\Theta_r = 1$, 3, and 10 choosing cork temperature $\Theta_c = 0.06$ (left panel) and $\Theta_c = 0.06$, 0.3, and 0.4 keeping $\Theta_r = 3$ (right panel). In both panels, the overplotted dotted curves are the corresponding smoothed spectra by applying the Savitzky–Golay filter. Second row: variation of α with Θ_r (left) and Θ_c (right). Third row: β as a function of Θ_r (left) and Θ_c (right). In the bottom row, dependence of $\varepsilon_{\text{peak}}$ is shown upon Θ_r (left panel) and Θ_c (right panel). For all the panels, $\theta_{\text{obs}} = 0.105$ rad, $\theta_j = 0.1$ rad, and $\gamma = 20$.

column of Figure 5. As Θ_c increases from 0.06 to 0.4, α varies from -1.9 to -1.55, β changes from -3.0 to -2.4, and $\varepsilon_{\text{peak}}$ covers a large range between 187 KeV and 1.19 MeV. All these values are within the observed ranges seen in GRB prompt phase observations.

5. Summary

In this Letter we have considered Comptonized pair equilibrium and bremsstrahlung spectra near the center of the star when a gamma-ray burst takes place. These seed photons interact with a radially expanding stellar cork outside the stellar surface and are

backscattered after undergoing Compton scattering with the relativistic electrons within the cork. The backscattered photons are then observed by an observer situated at angle θ_{obs} from the jet axis.

The obtained spectra have a negative low-energy photon index α and steeper high-energy photon index β. Our model predicts a large range of parameters $\alpha = -1.95$ to -1.1, $\beta = -3.5$ to ~ -2.4, and $\varepsilon_{peak} = $ a few KeV to a few tens of MeV. In the observed surveys, the peak values of low- and high-energy photon indices for the GRB population are obtained to be $\alpha = -1$ $\beta \sim -2.5$ and $\varepsilon_{peak} \sim 1$ MeV (Preece et al. 2000; Kaneko et al. 2006; Ghirlanda et al. 2011; Pe'er 2015) with a large variation of their respective ranges in the GRB population. The obtained ranges of all the spectral parameters that govern the GRB prompt phase spectra are consistent with the observed ranges. Hence, the modification makes the spectra in the backscattering model consistent with observations keeping all other findings in VPE21 unchanged. In future works, we will shed light on the analytic understanding of the high-energy photon indices β and their dependence on physical parameters of the system. The evolution of pair plasma by expansion and subsequent emission of low-energy seed photons can potentially contribute to the afterglow that we aim at examining further.

ORCID iDs

Mukesh K. Vyas ● https://orcid.org/0000-0001-6560-0902
Asaf Pe'er ● https://orcid.org/0000-0001-8667-0889
David Eichler ● https://orcid.org/0000-0002-9051-9927

References

Amati, L. 2006, MNRAS, 372, 233
Brainerd, J. J. 1994, ApJ, 428, 21
Daigne, F., Bošnjak, Ž., & Dubus, G. 2011, A&A, 526, A110
Eichler, D. 2014, ApJL, 787, L32
Eichler, D. 2018, ApJL, 869, L4
Eichler, D., & Manis, H. 2008, ApJL, 689, L85
Farinelli, R., Basak, R., Amati, L., Guidorzi, C., & Frontera, F. 2021, MNRAS, 501, 5723
Ghirlanda, G., Ghisellini, G., & Nava, L. 2011, MNRAS, 418, L109
Globus, N., & Levinson, A. 2014, ApJ, 796, 26
Goodman, J. 1986, ApJL, 308, L47
Gruber, D., Greiner, J., von Kienlin, A., et al. 2011, A&A, 531, A20
Kaneko, Y., Preece, R. D., Briggs, M. S., et al. 2006, ApJS, 166, 298
Kumar, P., & Zhang, B. 2015, PhR, 561, 1
Levinson, A., & Eichler, D. 1993, ApJ, 418, 386
Levinson, A., & Eichler, D. 2003, ApJL, 594, L19
Levinson, A., & Globus, N. 2013, ApJ, 770, 159
López-Cámara, D., Morsony, B. J., Begelman, M. C., & Lazzati, D. 2013, ApJ, 767, 19
MacFadyen, A. I., & Woosley, S. E. 1999, ApJ, 524, 262
McKinney, J. C. 2005a, arXiv:astro-ph/0506368
McKinney, J. C. 2005b, arXiv:astro-ph/0506369
Meszaros, P., Laguna, P., & Rees, M. J. 1993, ApJ, 415, 181
Nagakura, H., Hotokezaka, K., Sekiguchi, Y., Shibata, M., & Ioka, K. 2014, ApJL, 784, L28
Nakar, E., & Piran, T. 2017, ApJ, 834, 28
Paczynski, B. 1986, ApJL, 308, L43
Pe'er, A. 2015, AdAst, 2015, 907321
Pilla, R. P., & Loeb, A. 1998, ApJL, 494, L167
Popham, R., Woosley, S. E., & Fryer, C. 1999, ApJ, 518, 356
Preece, R. D., Briggs, M. S., Mallozzi, R. S., et al. 2000, ApJS, 126, 19
Ramirez-Ruiz, E., MacFadyen, A. I., & Lazzati, D. 2002, MNRAS, 331, 197
Tavani, M. 1996, ApJ, 466, 768
Vyas, M. K., Pe'er, A., & Eichler, D. 2021, ApJ, 908, 9
Waxman, E., & Mészáros, P. 2003, ApJ, 584, 390
Woosley, S. E. 1993a, AAS Meeting Abstracts, 182, 55.05
Woosley, S. E. 1993b, ApJ, 405, 273
Zdziarski, A. 1984, PhST, 7, 124
Zhang, W., Woosley, S. E., & Heger, A. 2004, ApJ, 608, 365
Zhang, W., Woosley, S. E., & MacFadyen, A. I. 2003, ApJ, 586, 356